Taxol induces caspase-independent cytoplasmic vacuolization and cell death through endoplasmic reticulum (ER) swelling in ASTC-a-1 cells

Tong-sheng Chen [a,*], Xiao-ping Wang [b], Lei Sun [a], Long-xiang Wang [a], Da Xing [a,*], Martin Mok [c]

[a] *MOE Key Laboratory of Laser Life Science & Institute of Laser Life Science, South China Normal University, Guangzhou 510631, China*
[b] *Department of Anesthesiology, The First Affiliated Hospital of Jinan University, Guangzhou 510632, China*
[c] *Department of Anesthesiology, University of Southern California, Los Angeles, CA 90033, USA*

Abstract

High concentration of taxol was found to induce programmed cell death (PCD) and cytoplasm vacuolization in human lung adenocarcinoma (ASTC-a-1) cells. To elucidate the relationship between the PCD and cytoplasm vacuolization, confocal fluorescence microscopy was performed on the cytoplasm vacuolization, endoplasmic reticulum (ER) and mitochondria swelling after taxol treatment in living cells. erRFP plasmid was used to probe the ER distribution, and SCAT3 plasmid was used to monitor the caspase-3 activation in living cells. Our results showed that taxol induced concentration-dependent and caspases-independent cytoplasm vacuolization and cell death through ER and mitochondria swelling. Live confocal imaging of ASTC-a-1 cells stably expressing SCAT3 further verified that taxol-induced cytoplasm vacuolization and cell death was caspase-3-independent. In conclusion, we found for the first time that taxol induces a paraptosis-like PCD in the ASTC-a-1 cells by cytoplasm vacuolization due to the swelling of both ER and mitochondria without activating the caspase enzymes.

Keywords: Taxol; Cytoplasm vacuolization; Programmed cell death (PCD); Caspases; Endoplasmic reticulum (ER)

1. Introduction

Taxol (paclitaxel), a chemotherapeutic agents, is effective against several kinds of tumors including ovarian, breast, non-small-cell lung tumors, and some head and neck carcinomas [1,2]. The exact mechanism of the cytotoxicity of taxol against tumor cells is still under extensive study [3–5]. Although it has been recognized that taxol-induced mitotic arrest results in apoptotic cell death, the biochemical events

linking microtubule binding to cell apoptosis are not well understood. Previous reports suggest that cell death may result from a novel action of taxol, which is independent of the microtubules [6,7], and taxol-induced apoptosis can be triggered through different mechanisms depending on cell cycle stage [8]. Huang et al. [9] also showed that taxol-induced mitotic arrest was independent of apoptotic cell death, and that taxol-induced mitotic arrest may not always be followed by apoptotic cell death. Different concentrations of taxol can trigger distinct effects on both the cellular microtubule network and biochemical pathways [10]. It is known that low concentrations of taxol (5–30 nM) alter microtubule dynamics and/or induce G2/M cell cycle arrest, whereas high concentrations of this drug (0.2–30 μM) cause significant microtubule damage [11]. However, recent studies showed that taxol may trigger cell death mainly via a currently unidentified caspases-independent and cell type-dependent mechanism in which the basic apoptotic machinery is merely co-activated [12–14], and that taxol induces necrosis in human endothelial cells as well as apoptosis and oncosis [8,15]. Recent studies also showed that calpain, JNK, P38 and c-FLIP play an important role in taxol-induced programmed cell death (PCD) [4,5,16].

Cell death has been divided into two main types: PCD, in which the cell plays an active role in its own demise, and passive (necrotic) cell death [17,18]. The PCD observed during development and tissue homeostasis has been classified morphologically into three main types [18]: type 1, also known as nuclear or apoptotic; type 2 or autophagic; and type 3, a non-lysosomal vacuolated degeneration. Apoptosis is the best characterized type of PCD with cells displaying membrane bleb, loss of the asymmetry of phosphatidyl-serine (PS) in the plasma membrane, nuclear fragmentation, and activation of caspases [19]. Type 3 cell death, also being called paraptosis [20], has been characterized by cytoplasmic vacuolization that begins with progressive swelling of mitochondria and endoplasmic reticulum (ER). Paraptosis typically does not respond to caspase inhibitors nor does it involve activation of caspases, formation of apoptotic bodies, or other characteristics of apoptotic morphology [17,18,20]. In contrast to apoptosis, Bcl-X_L is also not involved in the PCD in paraptosis [17,18,20].

Confocal fluorescence imaging and fluorescence resonance energy transfer (FRET) technology have been widely used to study protein-protein interactions in living cells [21–23]. SCAT3 is a FRET indicator of caspase-3 activation [21], which is composed of enhanced cyan fluorescence protein (ECFP) as the FRET donor and Venus, a variant of enhanced yellow fluorescence protein (EYFP), as the FRET acceptor, linked by peptides containing the caspase-3 cleavage sequence, DEVD [21]. This sequence is found in many cytosolic and nuclear caspase substrates and is cleaved by several effector caspases including caspase-3 and caspase-7 [21]. Caspase-3 is believed to play a central role in the execution of apoptosis, because this enzyme is required for oligonucleosomal DNA fragmentation and it promotes the activation of other effector caspases [21]. Our previous study used the human lung cancer (ASTC-a-1) cell line stably expressing SCAT3 to study caspase-3 activation by alkaline condition [23] in living cells. Klee et al. [22] constructed an erRFP plasmid, which specifically targets the endoplasmic reticulum (ER) lumen, to study the role of Bcl-xL and Bak in single living cell.

The present study used confocal fluorescence imaging and FRET technology to study the mechanism of taxol-induced cytoplasm vacuolization, ER and mitochondria swelling in living ASTC-a-1 cells. As far as we know this would be the first reported study of this kind.

2. Materials and methods

2.1. Cell lines

ASTC-a-1 cells were grown in DMEM supplemented with 10% fetal calf serum (FCS), and the cells were maintained at 37 °C in a humidified atmosphere (95% air and 5% CO_2) at pH 7.4.

2.2. Reagents

Dulbecco's modified Eagle's medium (DMEM) was purchased from GIBCO (Grand Island, NY). Lipofectamine 2000 was purchased from Invitrogen (Carlsbad, CA). DNA Extraction kit was purchased from Qiagen (Valencia, CA). SCAT3 was provided by Professor Masayuki Miura [21], and erRFP was provided by Professor Pimentel-Muiños [22]. z-VAD-fmk, caspase-family broad spectra inhibitor, was purchased from BioVision (USA). Taxol was purchased from Haikou Pharmaceutical Co. Ltd. (Haikou, China).

2.3. Cell proliferation assay

Cell viability assays were performed using Cell Counting Kit-8 (CCK-8) (WST-8, Dojindo, Japan), according to the supplier recommendations [23]. Absorbance was

measured at 450 nm using auto microplate reader (infinite M200, Tecan, Austria). Cell viability was expressed as the percentage of viable cells relative to untreated cells using the absorbance at 450 nm. All experiments were performed in quintuplicate from three separate occasions.

2.4. Cell transfection and screening

ASTC-a-1 cells were cultured in DMEM supplemented with 10% serum at a density of 4×10^3 cells/well in 35 mm glass dish. After 24 h, when the cells reached 30–50% confluence in DMEM containing 10% FBS at 37 °C in 5% CO_2, plasmid DNA of GFP and erRFP were transfected into the cells by using Lipofectamine 2000. Serum-free medium of 0.8 ml was added to the tube containing the Lipofectamine 2000. After 5–24 h, the medium containing DNA was replaced with 2 ml of DMEM containing FBS. After 24–48 h, the cells can be used for experiments. The cells stably expressing SCAT3 reporter were screened with 0.8 mg/ml G418, and positive clones were picked up with micropipettes [23].

2.5. Confocal fluorescence live monitoring

Fluorescence confocal imaging and FRET were done on a confocal microscope system with C-Apochromat 40× NA 1.3 and 100× 1.4 NA oil objective (Carl Zeiss Inc., Germany). The excitation wavelengths were 458 nm for SCAT3 and CFP-Bid, 514 nm for Venus, 543 nm for erRFP (Red GFP), 488 nm for GFP. The emission fluorescence channels were 470–500 nm for CFP, 500–550 nm for GFP, 530 nm long pass for Venus, 600 nm long pass for erRFP. To quantify the results, the images of CFP and Venus emission intensities were processed with Zeiss Rel 3.2 image processing software (Zeiss Inc., Germany).

2.6. Hoechst 33258 and rhodamine123 staining

Cells were grown on the coverslip of a 35 mm chamber. After being washed with PBS three times, cells were stained with 1 μM Hoechst 33258 for 15 min at room temperature. The cells were then washed three times with PBS and the images were recorded using a digital camera (Nikon, Tokyo, Japan) with 1280 × 1280 pixels resolution. Cells were washed with PBS three times, and stained with rhodamine 123 at 5 μM for 20 min in the dark at room temperature. The fluorescence images of cells stained with rhodamine 123 were measured by confocal microscope (Zeiss, Germany) after being washed with PBS three times.

2.7. Measurement of mitochondrial membrane potential ($\Delta\psi_m$)

Rhodamine 123 was used to evaluate changes in mitochondrial membrane potential. Cell suspensions (1×10^6) were incubated for 15 min at 37 °C in 1 ml PBS containing 1 μM rhodamine 123 and subsequently analyzed with a flow cytometer (FCM) (FACS, Arla BD, USA). Results were expressed as the proportion of cells exhibiting high mitochondrial membrane potential which was estimated by reduced fluorescence intensity from rhodamine 123.

2.8. FRET and acceptor photobleaching

Acceptor photobleaching experiments were carried out to assess the correct expression and the cleavage of the SCAT3 plasmid in single living cell as reported in our previous report [23]. The acceptor (Venus) in the region of chosen cell was selectively bleached with the maximum of 514 nm laser line. Upon photobleaching there was a marked decrease of the acceptor fluorescence (Venus), which coincided with an increase of the donor fluorescence (CFP).

2.9. Monitoring of emission spectra of SCAT3 inside living cells

Each well of 96-well plate contained 1×10^6 cells stably expressing SCAT3. The emission spectra of SCAT3 inside living cells were scanned using auto microplate reader (infinite M200, Tecan, Austria). The excitation wavelengths were 406–446 nm, and the emission spectra were 454–600 nm. The scanning step was 2 nm.

2.10. Statistics

Experiments are the means of five-plicates, and each experiment was done five times. Data are expressed as means ± SD. Statistical analyses were performed with SPSS12 (SPSS, Chicago) by using the two-sample t-test. Differences were considered statistically significant when $P \leqslant 0.05$.

3. Results

3.1. Taxol inhibits cell viability independent of caspase

Cell viability was performed by CCK-8 assay after the cells were exposed to various concentration of taxol for 24 h. Our results demonstrated that taxol at greater than 30 μM induced significantly cell death (Fig. 1A). We also assessed the effect of z-VAD-fmk, a caspase-family broad spectra inhibitor, on the taxol-induced cell death. The cells were treated with 2 μM z-VAD-fmk 1 h before 70 μM taxol treatment according to the manufacturer. Our results showed that incubation of the cells with z-VAD-fmk in addition to taxol did not significantly decrease the inhibition effect of taxol compared with taxol alone at both 12 and 24 h after taxol treatment (Fig. 1B), implying that caspases were not involved in the taxol-
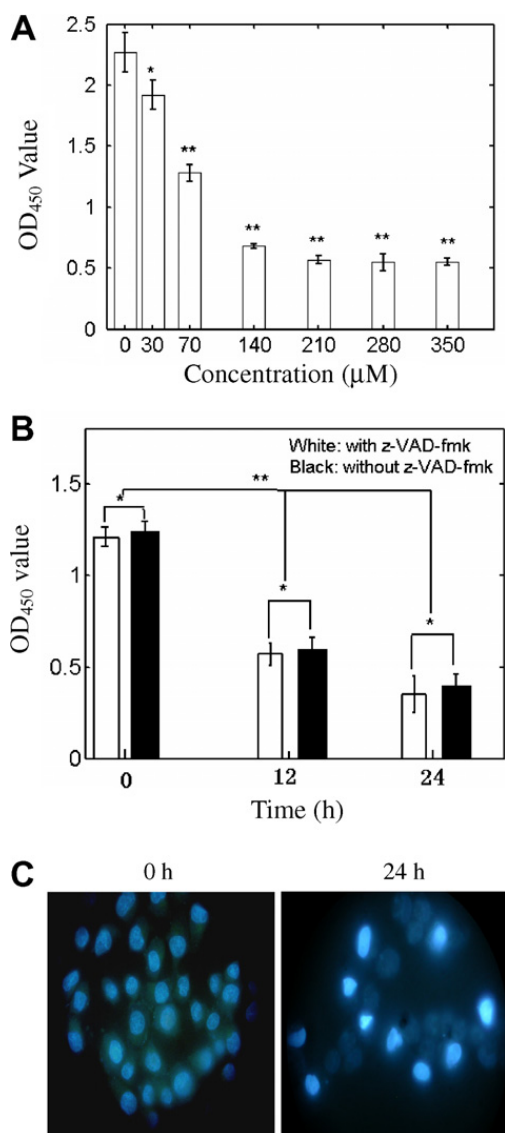
Fig. 1. Effects of taxol on cell viability. (A) Taxol-induced concentration-dependent cell death 24 h after taxol treatment, $^{*}P < 0.05$, and $^{**}P < 0.01$, and (B) effects of z-VAD-fmk, a broad spectra caspases inhibitor, on the cell viability at 12 and 24 h after 70 μM taxol treatment, $^{*}P < 0.1$, and $^{**}P < 0.01$. Results are an average of quintuplicate experiments and the standard deviation (SD) is shown in a bar. (C) Hoechst 333258 fluorescence images of cells at time 0 and 24 h after 70 μM taxol treatment (magnification 1000×).

induced cell death. Hoechst333258 staining results showed that taxol induced slight nuclear condensation (Fig. 1C) at 24 h after 70 μM taxol treatment.

3.2. Taxol induces cytoplasm vacuolization through ER vacuolization

To assess the effect of taxol on the cytoplasm vacuolization, the cells expressing GFP were imaged using confocal fluorescence microscope at 24 h after treatment with various concentrations of taxol. We found that significant cyto-

plasm vacuolization was induced by taxol (Fig. 2A), and the vacuolization proportion of cells with GFP fluorescence increased in a concentration-dependent fashion (Fig. 2B). We next performed the effect of z-VAD-fmk on the taxol-induced cytoplasm vacuolization. Our results showed that z-VAD-fmk treatment did not increase the proportion of vacuolated cells (Fig. 2C), implying that caspases are not necessary for taxol-induced cytoplasm vacuolization.

To assess if the taxol-induced cytoplasm vacuolization were topologically related to ER, cells were co-expressed with both GFP and erRFP plasmids. The erRFP plasmid can specifically probe ER [22]. Our results verified that ER distribution was in net fashion in healthy cells (Fig. 2D). However, 24 h after 70 μM taxol treatment, confocal imaging showed that taxol-induced cytoplasm vacuolization were filled with the co-expressed erRFP (Fig. 2E), and the taxol-induced dead cells were filled completely with erRFP (indicated by arrow in Fig. 2E). These results showed that taxol-induced cytoplasm vacuolization was mainly due to the ER swelling.

3.3. Loss of mitochondrial membrane potential ($\Delta\psi_m$) and mitochondria swelling induced by taxol

Mitochondria play central roles in the regulation of both apoptotic and non-apoptotic cell death [5,20]. We used FCM to examine the involvement of mitochondria in taxol-induced cell death by monitoring $\Delta\psi_m$ at 0, 12 and 24 h after 70 μM taxol treatment (Fig. 3A). The percent of cells with rhodamine123 fluorescence were 88.2%, 54.1% and 29.5% at 0, 12 and 24 h after taxol treatment, respectively, implying that taxol induced the loss of mitochondrial membrane potential ($\Delta\psi_m$).

In order to determine whether taxol induces mitochondria swelling, we used confocal fluorescence microscope to image the mitochondria by rhodamine123 staining. Fig. 3B shows a typical fluorescence image of mitochondria inside living cells. Taxol deceased significantly the number of mitochondria, and induced mitochondria swelling (Fig. 3B). Dynamics of increasing mitochondria size induced by taxol were recorded using confocal microscope, and the statistical results of mitochondria size after taxol treatment are shown in Fig. 3C. Taxol induced significant mitochondria swelling 6 h after treatment (Fig. 3C). The mitochondria size was 0.76 ± 0.14 μm, 1.11 ± 0.15 μm, 1.09 ± 0.19 μm and 1.40 ± 0.50 μm at 0, 6, 10 and 18 h after taxol treatment, respectively. These results suggested that some of the cytoplasm vacuolization induced by taxol might be derived from the mitochondria swelling.

3.4. Taxol-induced caspase-3-independent cytoplasm vacuolization

In our previous studies, we demonstrated that the SCAT3 distributed evenly in both the nuclei and the cytoplasm [23]. The live FRET imaging of the cells
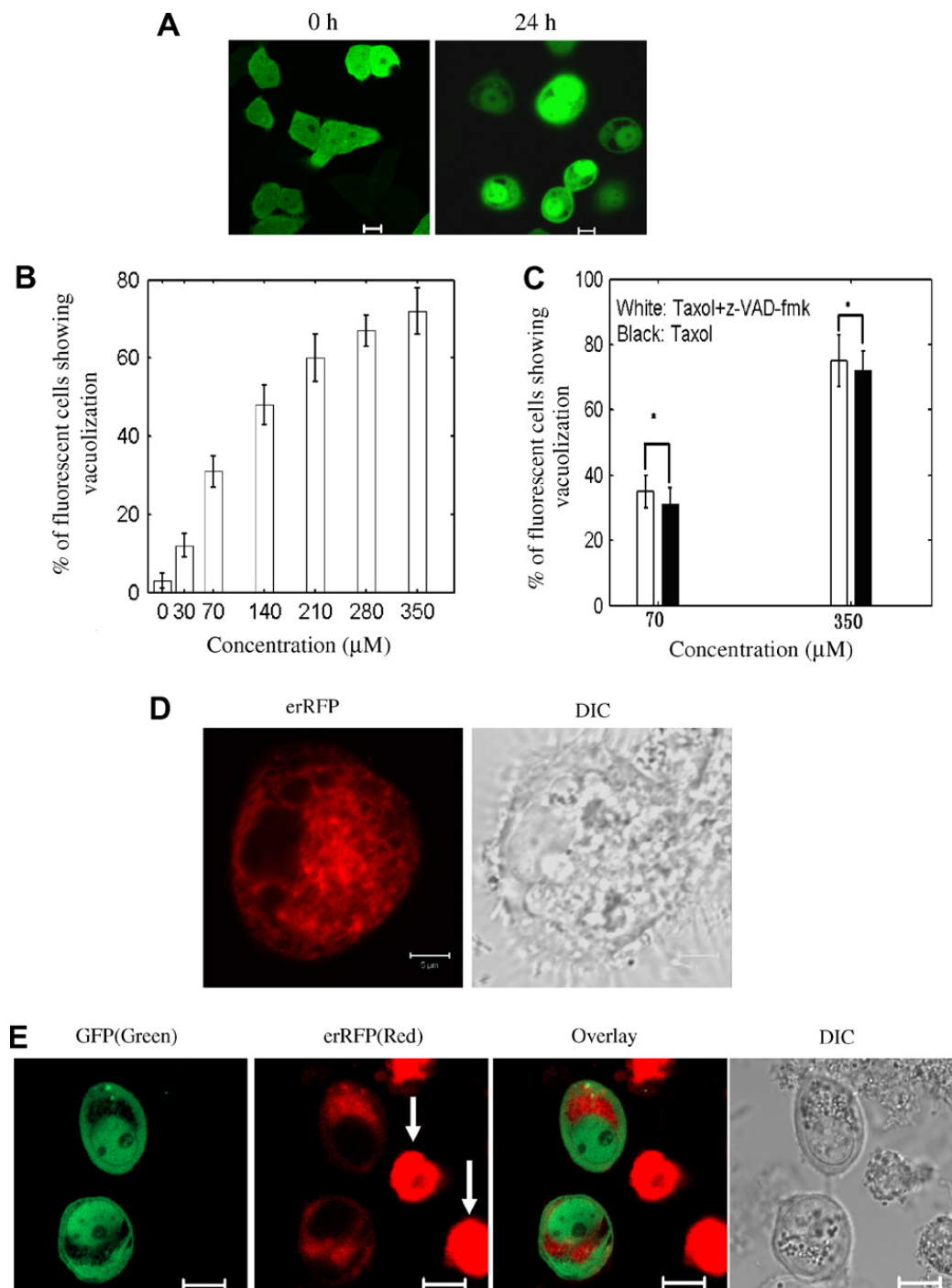
Fig. 2. Taxol-induced cytoplasm vacuolization. (A) Fluorescence images of cells expressing GFP at time 0 h and 24 h after 70 μM taxol treatment. Scale bar: 10 μM. (B) Vacuolization proportion of cells showing GFP fluorescence 24 h after taxol with different concentrations. The number of cells is 200, 210, 160, 120, 110, 130 and 100 from three-independent groups for the 0, 30, 70, 140, 210, 280 and 350 μM, respectively. (C) Effects of z-VAD-fmk on the vacuolization proportion at 24 h after 70 and 350 μM of taxol treatment, respectively. (D) A typical fluorescence image of cell expressing erRFP without any treatment. Scale bar: 5 μM. (E) Fluorescence images of cells coexpressing both GFP and erRFP 24 h after 70 μM taxol treatment. GFP (green) shows the morphological changes, and erRFP (red) shows the ER localization. The two cells indicated by white arrows are dead. Scale bar: 10 μM. (For interpretation of color mentioned in this figure the reader is referred to the web version of the article.)

stably expressing SCAT3 was done in single living cells after taxol treatment by time-lapse confocal fluorescence microscope. Fig. 4A shows typical fluorescence series images of a cell stably expressing SCAT3 for

the CFP (BP470 500 nm) and Venus (LP 530 nm) channels after 70 μM taxol treatment. Cytoplasm vacuolization also occurred (Fig. 4A), which is consistent with the aforementioned results (Fig. 2). Fig. 4B shows
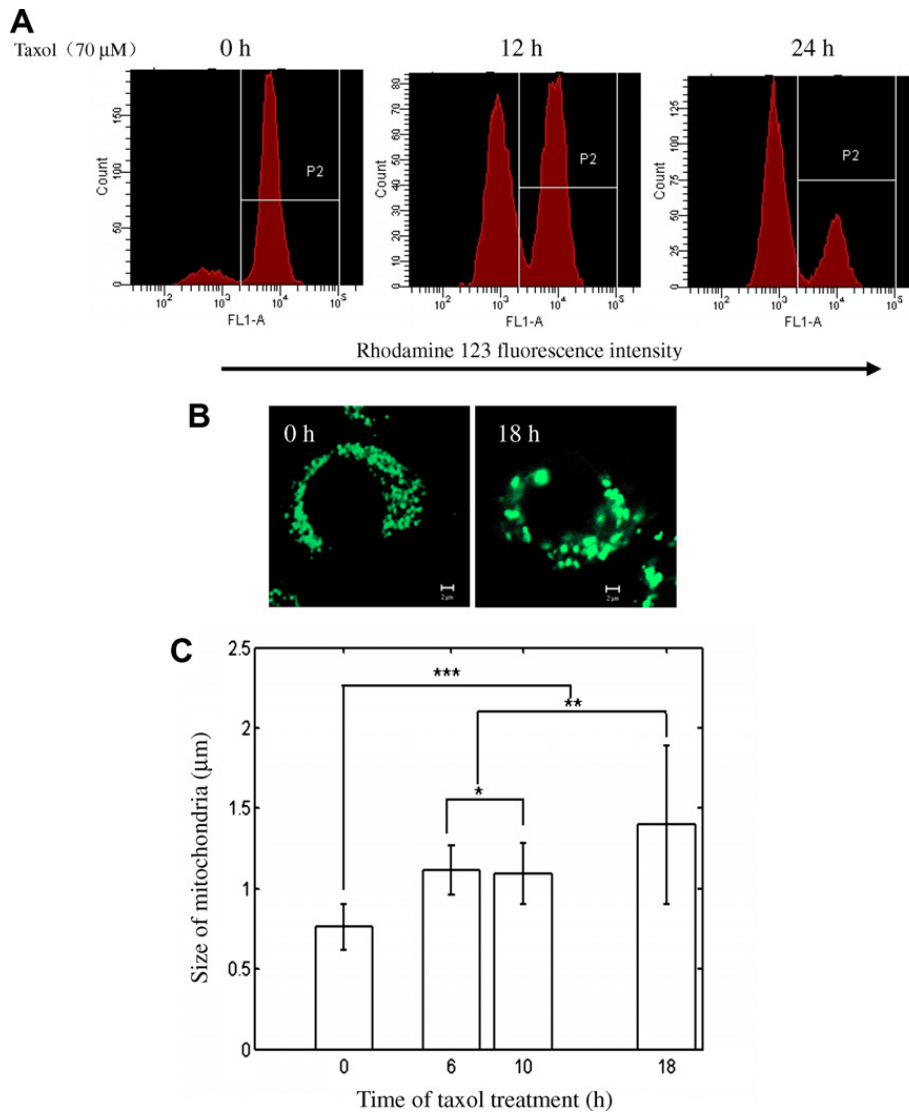
Fig. 3. Taxol-induced mitochondria swelling. (A) Seventy micromolar taxol treated cells were subjected to mitochondrial transmembrane potential assessment 24 h after treatment. (B) Typical fluorescence images of mitochondria at 0 and 18 h after 70 μM taxol treatment. Scaled bar: 2 μm. (C) Quantitative results of mitochondria size at 0, 6, 10 and 18 h after taxol treatment. The number of mitochondria is at least 70 from three-independent groups.

the corresponding dynamics of the ratio of Venus/CFP for eight-independent cells. For direct comparisons, the initial intensities of all channels were modified to 1. Despite taxol-induced cytoplasm vacuolization (Fig. 4A), the ratio of Venus/CFP was almost constant within 21 h (Fig. 4B), implying that caspase-3 was not activated.

To further confirm whether caspase-3 was involved in the taxol-induced cytoplasm vacuolization and cell death in ASTC-a-1 cells, acceptor photobleaching was done in the cells shown in Fig. 4A at 21 h after 70 μM taxol treatment, same as our previous study [23]. Photobleaching Venus induced decrease of fluorescence intensity in Venus channel, while the fluorescence intensity in the CFP channel increased markedly (Fig. 4C), implying that the taxol did not induce caspase-3 activation.

We next detected the emission spectra of SCAT3 inside living cells at 24 h after 70 μM taxol treatment with and without z-VAD-fmk using auto microplate reader (infinite M200, Tecan, Austria) (Fig. 4D). Comparing control with 24 h after taxol treatment, the emission spectra of SCAT3 were independent of taxol and z-VAD-fmk (Fig. 4D), further indicating that caspases were not activated by taxol.

4. Discussion

There is increasing evidence of the chemotherapeutic potential of taxol in the treatment of a variety of cancers. However, the molecular mechanism of taxol-induced cell death is still controversial. Taxol can induce caspases-dependent and caspase-inde-
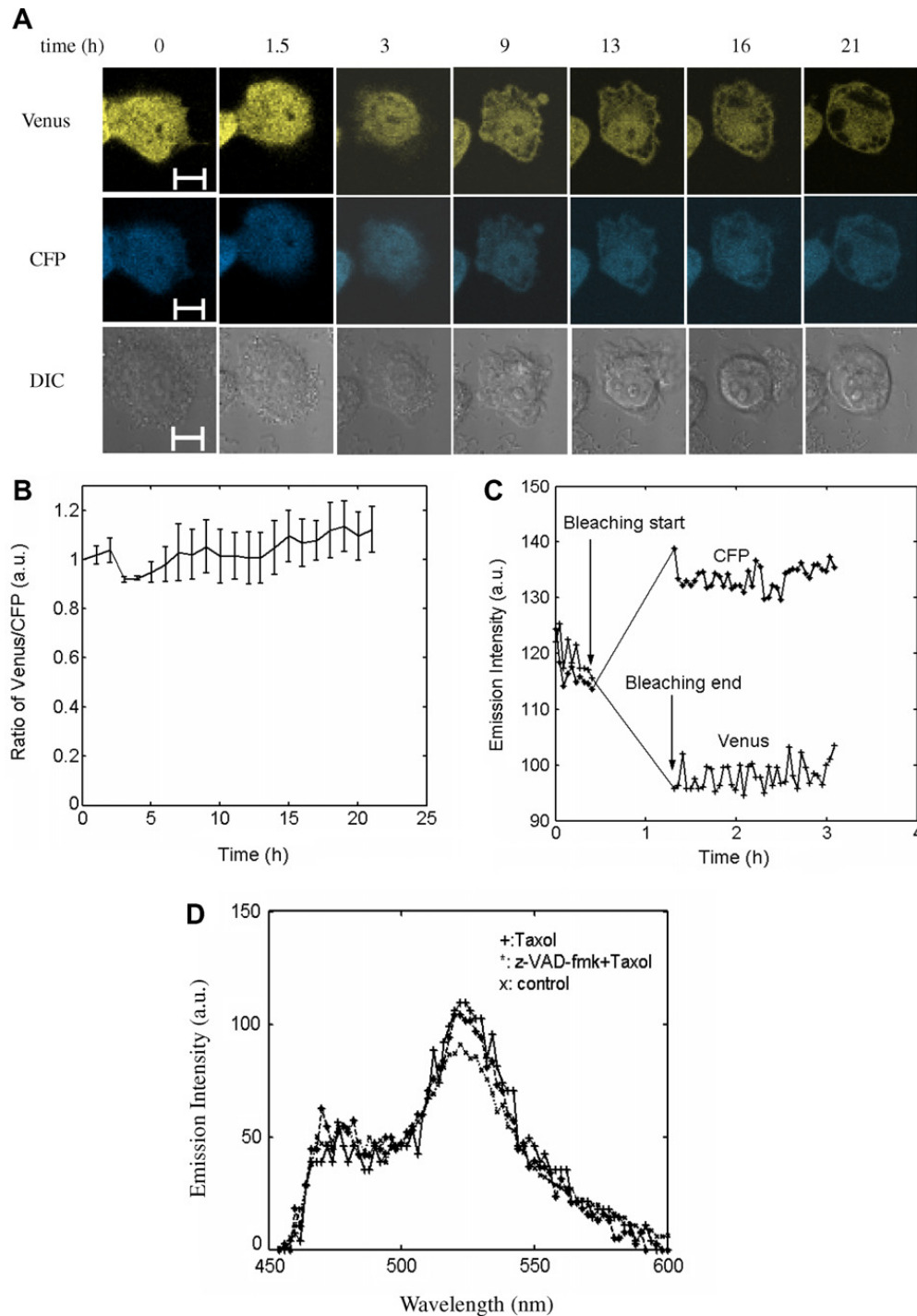
Fig. 4. Kinetics of caspase-3 activation and morphological change after 70 mM taxol treatment. (A) Confocal image series of a typical cell stably expressing SCAT3 in both Venus and CFP channels. Scaled bar: 10 mm. (B) Dynamics of the ratio of Venus/CFP from eight-independent cells. (C) Acceptor (Venus) photobleaching for the cell in (A) at 21 h after taxol treatment. The Venus was photobleached by the maximum of 514 nm laser. The fluorescence intensity of CFP channel increases during Venus photobleaching. (D) Emission spectra analysis of SCAT3 inside living cells at 24 h after taxol treatment with and without z-VAD-fmk.

pendent cell apoptosis [12–14], and can also induce necrosis [8,14]. In this report we for the first time demonstrated that taxol at high concentration (>30 μM) induced concentration-dependent and caspases-independent cell death and cytoplasm vac-

uolization though ER and mitochondria swelling without apoptotic bodies and membrane disruption within 24 h.

In the present study, we monitored the dynamics of cell morphological change after 70 μM taxol

treatment, and taxol was found to induce cells swelling due to the ER vacuolization at 3–15 h after treatment. However, most of the cells at 18 h after taxol treatment appeared to have membrane bleb and shrinkage, which may be due to the ER shrinkage (Fig. 2D), but no apoptotic bodies (Fig. 4A). To determine whether taxol induced cell necrosis, we assessed the effect of PI staining on the cell membrane at 24 h after 70 μM taxol treatment (data no shown), and the results showed that taxol did not induce membrane disruption, implying that taxol did not induce cell necrosis within 24 h. We also found that the taxol-induced cell death and cytoplasm vacuolization were concentration-dependent and caspases-independent. Dynamical monitoring of caspase-3 activation inside living cells showed that taxol did not decrease but increase the FRET efficiency of SCAT3 (Fig. 4). This change in FRET efficiency may be due to the conformational change of SCAT3 or the changes of fluorescence characteristics of both the CFP and Venus by taxol-induced environment changes inside the cells. These results suggested that taxol at high concentration induced a novel alternative PCD resembling the paraptosis [17,18] in ASTC-a-1 cells.

In addition to cell type specificity, the fate of cells following taxol treatment may depend on concentration of taxol [6,8,24]. In culture cells, high concentration of taxol had been shown to cause significant microtubule damage, which in turn induces caspases-independent PCD by regulating gene expression such as Bak, Bax and cyclin B1[11]. High concentration of taxol also activates kinases such as c-Jun-N-terminal kinase/stress-activated protein kinases (JNK/SAPK) [25] and others [11]. Bak and Bax proteins also reside in the ER in addition to their mitochondrial localization [26]. Taxol-induced microtubule damage may trigger ER stress that induces Ca^{2+} depletion from the ER lumen, which may lead to ER swelling, and conformational changes and oligomerization of Bak and Bax on the ER membrane. The induction of JNK activation can lead to both PCD and necrosis [27]. Although cell swelling, ER swelling as well as mitochondria swelling were observed after taxol treatment in our study, PI staining, however, showed no cell membrane disruption which indicates that taxol-induced cell death is PCD and not necrosis. It still remains unclear, however, whether microtubule damage is directly responsible for the high concentration of taxol-induced ER and mitochondria swelling, which awaits further study.

The taxol-induced ER vacuolization in this report may be mediated by the formation of a molecular complex simultaneously including Bak and Bcl-X_L. In contrast to its effect at low concentration, taxol at high concentration may increase rapidly the level of some cell death factors such as Bcl-X_L, Bak and Bax, etc. [11,28]. In turn, the interaction between these factors may induce ER vacuolization. Previous reports had suggested that treatment with taxol dose-dependently increases the level of Bcl-X_L [28], which can induce ER vacuolization via Bak [22], and this stimulating effect should be caspases-independent. ER is one of the main calcium storages in the cell [26], and some PCD stimuli can promote calcium release from ER store thus leading to cell death [26,29].

In addition, the mitochondria swelling described here may be due to the taxol-induced mitochondria stress. Taxol at high concentration may increase greatly the production of reactive oxygen species (ROS) in mitochondria [5]. The high ROS generation would lead to the loss of mitochondrial membrane potential and the mitochondrial membrane permeability. In turn, the taxol-induced high osmotic pressure by an inward ionic current induces mitochondria swelling.

In conclusion, live fluorescence imaging in living cells clearly showed that taxol induced cell death and cytoplasm vacuolization through ER and mitochondria swelling, which was concentration-dependent and caspases-independent. Understanding the molecular mechanism of this novel alternative PCD may help us in the development of cancer therapy in the future.

Acknowledgements

References

[1] A.L. Fields, C.D. Runowicz, Current therapies in ovarian cancer, Cancer Invest. 21 (2003) 148–156.

[2] J. Crown, M. O'Leary, W.S. Ooi, Docetaxel and paclitaxel in the treatment of breast cancer: a review of clinical experience, Oncologist 9 (Suppl. 2) (2004) 24–32.

[3] W.T.W. Day, F. Najafi, C.H. Wu, A.R. Safa, Cellular FLICE-like inhibitory protein (c-FLIP): a novel target for

taxol-induced apoptosis, Biochem. Pharmacol. 71 (2006) 1551–1561.

[4] N.A.N. Shajahan, A. Wang, M. Decker, R.D. Minshall, M.C. Liu, R. Clarke, Caveolin-1 tyrosine phosphorylation enhances paclitaxel-mediated cytotoxicity, J. Biol. Chem. 282 (2007) 5934–5943.

[5] D. Selimovic, M. Hassan, Y. Haikel, U.R. Hengge, Taxol-induced mitochondrial stress in melanoma cells is mediated by activation of c-Jun N-terminal kinase (JNK) and p38 pathways via uncoupling protein 2, Cell. Signal. 20 (2008) 311–322.

[6] H.C.H. Lieu, Y.N. Chang, Y.K. Lai, Dual cytotoxic mechanisms of submicromolar taxol on human leukemia HL-60 cells, Biochem. Pharmacol. 53 (1997) 1587–1596.

[7] M.J.M. Dziadyk, M. Sui, X. Zhu, W. Fan, Paclitaxel-induced apoptosis may occur without a prior G2/M-phase arrest, Anticancer Res. 24 (2004) 27–36.

[8] C.P.C. Liao, C.H. Lieu, Cell cycle specific induction of apoptosis and necrosis by paclitaxel in the leukemic U937 cells, Life Sci. 76 (2005) 1623–1639.

[9] Y. Huang, Y. Fang, J.M. Dziadyk, J.S. Norris, W. Fan, The possible correlation between activation of NF-kappaB/IkappaB pathway and the susceptibility of tumor cells to paclitaxel-induced apoptosis, Oncol. Res. 13 (2002) 113–122.

[10] K. Torres, S.B. Horwitz, Mechanisms of taxol-induced cell death are concentration dependent, Cancer Res. 58 (1998) 3620–3626.

[11] T.H. Wang, H.S. Wang, Y.K. Soong, Paclitaxel-induced cell death: where the cell cycle and apoptosis come together, Cancer 88 (2000) 2619–2628.

[12] C. Huisman, C.G. Ferreira, L.E. Broker, J.A. Rodriguez, E.F. Smit, P.E. Postmus, F.A.E. Kruyt, G. Giaccone, Paclitaxel triggers cell death primarily via caspase-independent routes in the non-small cell lung cancer cell line NCI-H4601, Clin. Cancer Res. 596 (2002) 596–606.

[13] R. Ofir, R. Seidman, T. Rabinski, M. Krup, V. Yavelsky, Y. Weinstein, M. Wolfson, Taxol-induced apoptosis in human SKOV3 ovarian and MCF7 breast carcinoma cells is caspase-3 and caspase-9 independent, Cell Death Diff. 9 (2002) 636–642.

[14] S.J. Park, C.H. Wu, J.D. Gordon, X. Zhong, A. Emami, A.R. Safa, Taxol induces caspase-10-dependent apoptosis, J. Biol. Chem. 279 (2004) 51057–51067.

[15] A. Mailloux, K. Grenet, A. Bruneel, B. Beneteau-Burnat, M. Vaubourdolle, B. Baudin, Anticancer drugs induce necrosis of human endothelial cells involving both oncosis and apoptosis, Eur. J. Cell Biol. 80 (2001) 442–449.

[16] D. Piñeiro, M.E. Martín, N. Guerra, M. Salinas, V.M. González, Calpain inhibition stimulates caspase-dependent apoptosis induced by taxol in NIH3T3 cells, Exp. Cell Res. 313 (2007) 369–379.

[17] S. Sperandio, K. Poksay, I.D. Belle, M.J. Lafuente, B. Liu, J. Nasie, D.E. Bredesen, Paraptosis: mediation by MAP kinases and inhibition by AIP-1/Alix, Cell Death Differ. 11 (2004) 1066–1075.

[18] L.E. Bröker, F.A.E. Kruyt, G. Giaccone, Cell death independent of caspases: a review, Clin. Cancer Res. 11 (9) (2005) 3155–3162.

[19] N.A. Thornberry, Y. Lazebnik, Caspases: enemies within, Science 281 (1998) 1312–1316.

[20] S. Sperandio, L.D. Belle, D.E. Bredesen, An alternative, non-apoptotic form of programmed cell death[J], Proc. Natl. Acad. Sci. USA 26 (2000) 14376–14381.

[21] K. Takemoto, T. Nagai, A. Miyawaki, M. Miura, Spatio-temporal activation of caspase revealed by indicator that is insensitive to environmental effects, J. Cell Biol. 160 (2003) 235–243.

[22] M. Klee, F.X. Pimentel-Muinos, Bcl-XL specifically activates Bak to induce swelling and restructuring of the endoplasmic reticulum, J. Cell Biol. 168 (2005) 723–734.

[23] T.S. Chen, J.J. Wang, D. Xing, W.R. Chen, Spatio-temporal dynamic analysis of Bid activation and apoptosis induced by alkaline condition in human lung adenocarcinoma cell, Cell Physiol. Biochem. 20 (2007) 569–578.

[24] M.O. Trielli, P.R. Andreassen, F.B. Lacroix, R.L. Margolis, Differential taxol-dependent arrest of transformed and nontransformed cells in the G1 phase of the cell cycle, and specific related mortality of transformed cells, J. Cell Biol. 135 (1996) 689–700.

[25] L.F. Lee, G. Li, D.J. Templeton, J.P. Ting, Paclitaxel (taxol)-induced gene expression and cell death are both mediated by the activation of c-Jun NH2-terminal kinase (JNK/SAPK), J. Biol. Chem. 273 (1998) 28253–28260.

[26] W.X. Zong, C. Li, G. Hatzivassiliou, T. Lindsten, Q.C. Yu, J. Yuan, C.B. Thompson, Bax and Bak can localize to the endoplasmic reticulum to initiate apoptosis, J. Cell Biol. 162 (2003) 59–69.

[27] S. Papa, C. Bubici, F. Zazzeroni, C.G. Pham, C. Kuntzen, J.R. Knabb, K. Dean, G. Franzoso, The NF-κB-mediated control of the JNK cascade in the antagonism of programmed cell death in health and disease, Cell Death Differ. 13 (2006) 712–729.

[28] E. Chun, K.-Y. Lee, Bcl-2 and Bcl-X$_L$ are important for the induction paclitaxel resistance in human hepatocellular carcinoma cells, Biochem. Biophys. Res. Commun. 315 (2004) 771–779.

[29] R. Rizzuto, P. Pinton, D. Ferrari, M. Chami, G. Szabadkai, P.J. Magalhaes, F. Di Virgilio, T. Pozzan, Calcium and apoptosis: facts and hypotheses, Oncogene 22 (2003) 8619–8627.